Archives of Acoustics Vol. 50, No. 2, pp. 199–207 (2025), https://doi.org/10.24425/aoa.2025.154814

Research Paper

A Hybrid Method for Predicting the Bistatic Target Strength Based on the Monostatic Scattering Sound Pressure Data

Yuhang TANG(1), Chenyu FAN(1)*, Yinhao LI(2), Changxiong CHEN(2), Zilong PENG(2)

(1) *PLA Unit 92578*
Beijing, China

(2) *School of Energy and Power*
Jiangsu University of Science and Technology
Zhenjiang, China

*Corresponding Author e-mail: 15350715833@163.com

Received January 8, 2025; revised May 8, 2025; accepted May 10, 2025; published online June 16, 2025.

To predict the scattered acoustic field for underwater targets with separate transmission and reception points, a forecasting method based on limited scattered acoustic pressure data is proposed. This method represents the scattered acoustic field as the product of an acoustic scattering transfer function and a source density function. By performing numerical integration, the transfer function is obtained using the model surface grid information as input. An equation system concerning the unknown source density function is then derived using the computed scattering transfer matrix, the principle of acoustic reciprocity, and the geometric properties of the target. The unknown source density function is solved using the least squares method. The scattered field with separate transmission and reception points is then obtained by multiplying the calculated transfer matrix with the estimated source density function. This paper applies the finite element method (FEM) to solve the scattering field for a benchmark model with separate transmission and reception points. Using a subset of the elements as input, predictions of the omnidirectional scattered field were made. The predicted results were subsequently compared with those obtained from FEM simulations. The simulation results demonstrate that the proposed method maintains high computational accuracy and is applicable to the prediction of low-frequency scattered fields from underwater targets with spatially separated source and receiver. Further comparison with the FEM-calculated target strength patterns across varying incident–reception angles reveals a high level of agreement, indicating that accurate bistatic target strength predictions can be achieved with a limited amount of input data.

Keywords: acoustic scattering properties; bistatic scattering sound field; scattering sound field prediction; target strength.

1. Introduction

Acoustic waves are the only physical field capable of transmitting information effectively over long distances in the ocean. Devices that use acoustic waves for underwater detection, positioning, navigation, and communication are collectively referred to as sonar (Tang *et al.*, 2018). Currently, sonar technology and detection methods are undergoing significant transformation, with increasingly complex underwater acoustic environments. Future developments in sonar technology are expected to integrate active and passive systems, multi-band capabilities, and multifunctionality. Key directions include low-frequency, high-power, adaptive array processing, and distributed transmission and reception systems.

The rise of big data and artificial intelligence has also enabled the possibility of coordinated networks and formations of sonar-equipped tools, such as unmanned surface and underwater vehicles (UUVs). However, complex hull structures face unprecedented challenges from these three-dimensional underwater detection networks.

Research methods for studying the echo characteristics of complex hull structures can be categorized into theoretical solutions, numerical methods, and approximation methods. Theoretical solutions are primarily used to analyze the scattering acoustic fields of regular models, such as spheres and infinitely long cylinders. For more complex shapes and materials, numerical methods like the T-matrix method (Waterman, 2005), the finite element/boundary element method (FEM/BEM) (Zhou *et al.*, 2009), and the finite difference time domain (FDTD) method (Schneider *et al.*, 1998). Numerical methods offer a broad range of applications and are capable of solving target scattering problems under virtually any conditions. For high-frequency, large-scale models, the computational speed of numerical methods is often slow, necessitating the use of approximation methods for more efficient calculations. Fan and Zhou (2006) proposed a modified planar element method that incorporates considerations for occlusion and secondary scattering effects. Peng *et al.* (2018) presented a method to predict echo characteristics of surface targets using the Kirchhoff approximation. Xue *et al.* (2023) improved the computational efficiency of the patch element method by replacing planar elements with surface elements, thereby enhancing the overall calculation speed of the method.

The bistatic target detection offers advantages such as an excellent, wide detection range, and strong anti-jamming capability, leading many scholars to conduct in-depth studies on the bistatic acoustic scattering characteristics. Chen *et al.* (2024) proposed and validated a prediction method for underwater acoustic scattering. Liu *et al.* (2012) proposed a modification to the scattering integration region on the target surface, thereby extending the applicability of physical acoustics to arbitrary separation angles. Wang *et al.* (2022) developed a time-domain transformation method based on the Kirchhoff approximation for calculating bistatic acoustic scattering of underwater rigid targets. In the field of bistatic underwater maneuvering target tracking. Gunderson *et al.* (2017) discussed the interference and resonance structures present in the frequency responses of the targets, and presented bistatic spectra for a variety of elastic sphere materials. Meng *et al.* (2024) proposed a highlight model for predicting bistatic acoustic scattering characteristics. Schmidt (2001) studied bistatic scattering from buried targets in shallow water. Agounad *et al.* (2023) systematically analyzed the guided wave propagation characteristics of cylindrical shells under bistatic acoustic scattering configurations from both theoretical and experimental perspectives, and proposed a time–frequency analysis-based method to estimate the group velocities of waves propagating in different directions. Cheng *et al.* (2010) established a bistatic scattering strength model for underwater targets under far-field conditions based on the Kirchhoff approximation. Park *et al.* (2006) studied the bistatic acoustic scattering phenomena of a hemispherical closed cylinder. Gu *et al.* (2025) proposed an improved rapid prediction method for solving the full-space bistatic scattering acoustic field of underwater vehicles. Zhang *et al.* (2011) conducted a thorough review of the existing research, summarizing key advancements and trends in this area. Long *et al.* (2022) demonstrated through research that, in bistatic systems, detection performance for configurations such as quadrilateral, hexagonal, rhombic, and checkerboard layouts consistently outperforms that of collocated transmission and reception configurations. Schenck *et al.* (1995) developed a hybrid method to predict the complete three-dimensional acoustic scattering function from limited data by using computational models and least-squares problems. Currently, research on underwater bistatic scattering acoustic fields primarily focuses on typical configurations such as collocated transmission and reception, as well as forward scattering. There is relatively little research on the relationship between collocated and bistatic scattering fields. In early radar systems, a method known as the separation theorem was used to estimate the bistatic target strength based on the known monostatic target strength. However, the separation theorem is only applicable for small separation angles. There is currently no well-established method for calculating and relating the scattering echoes in bistatic systems.

This paper investigates the transmit-receive separation echo characteristics for large angles and omnidirectional scenarios, focusing on the prediction of transmit-receive separation scattering acoustic fields based on limited data. A prediction method for transmit-receive separation scattering acoustic fields is established, combining limited data, model geometry properties, numerical integration, acoustic reciprocity, and the least squares method. Using the integral formula of the acoustic field and the surface integral equation, the far-field scattering sound pressure is expressed as the product of the unknown sound source density function and the sound scattering transfer matrix. Through numerical integration, the target surface grid model is used as input to obtain the sound scattering transfer matrix. Based on the calculated sound scattering transfer matrix, the principle of acoustic reciprocity, and the geometric properties of the target, a system of equations for the unknown sound source density function is derived. The unknown density function is then solved using the least squares method. The

calculated sound scattering transfer matrix and the unknown sound source density function are multiplied to obtain the transmit-receive separation scattering acoustic field. The FEM is used to solve the transmit-receive separation scattering acoustic field for a Benchmark model. Several elements from the model are used as input to predict the omnidirectional transmit-receive separation scattering acoustic field. A comparison is made between the predicted results and the FEM results. The simulation results show that the method has good computational accuracy and can be used for calculating the transmit-receive separation scattering acoustic fields of complex underwater targets.

2. Theoretical method

The scattered acoustic field can be expressed as the product of the sound transfer function and the equivalent surface source density function of the target (Schenck *et al.*, 1995). As shown in Fig. 1, under the plane wave incidence from the direction $\widehat{\mathbf{x}}^{\mathrm{inc}}$, the sound pressure at the receiver point x can be expressed as

$$p^s\left(x,\widehat{\mathbf{x}}^{\mathrm{inc}}\right) = \frac{1}{4\pi}\int\limits_s q\left(\xi,\widehat{\mathbf{x}}^{\mathrm{inc}}\right)\left[\frac{\partial}{\partial n_\xi}+i\right] \cdot\frac{e^{-ikr(x,\xi)}}{r(x,\xi)}\,\mathrm{d}S(\xi), \tag{1}$$

where q is the unknown source density function; S represents the target surface; $\widehat{\mathbf{x}}^{\mathrm{inc}}$ is the unit vector in the direction of the incident point; ξ denotes a point on the target surface and $\widehat{\mathbf{n}}$ is the unit normal vector at a point on the target surface. Where $R(x)$ is the distance between the target and the receiver point in the far field, and $r(x,\xi)$ is the distance between a point ξ on the target surface and the receiver point in the near field. The target surface S is discretized into N_s surface elements, Eq. (1) is expressed as

$$p^s\left(x,\widehat{\mathbf{x}}^{\mathrm{inc}}\right) = \frac{1}{4\pi}\sum_{l=0}^{N_s} q_l(\widehat{\mathbf{x}}^{\mathrm{inc}})\int\limits_{s_0}\left[\frac{\partial}{\partial n_\xi}+i\right] \cdot\frac{e^{-ikr(x,\xi)}}{r\left(x,\xi\right)}\,\mathrm{d}S(\xi), \tag{2}$$

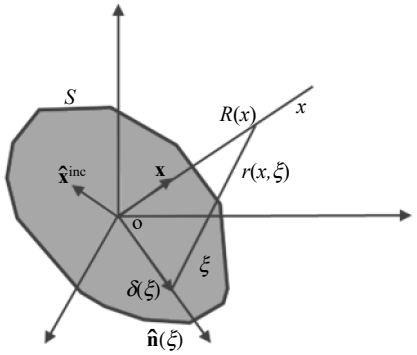

Fig. 1. Schematic diagram of target sound scattering.

when the receiver point x is defined in the far field of the integration surface S, $r(x,\xi)\doteq R(x)$ and divided by the spherical wave propagation factor $e^{-ikR(x)}/R(x)$, the far-field scattered sound pressure is defined as follows:

$$p^s_{ff}\left(x,\widehat{\mathbf{x}}^{\mathrm{inc}}\right) = \frac{1}{4\pi}\sum_{l=0}^{N_s} q(\widehat{\mathbf{x}}^{\mathrm{inc}}) \cdot\int\limits_S\left[ik\widehat{\mathbf{x}}\,\widehat{\mathbf{n}}(\xi)+i\right]e^{-ik\widehat{\mathbf{x}}\delta(\xi)}\,\mathrm{d}S(\xi). \tag{3}$$

Define the scattering acoustic field matrix $\mathbf{S}$, where the elements are denoted as $\mathrm{S}_{mn}=p^s_{ff}\left(\widehat{\mathbf{x}}_m,\widehat{\mathbf{x}}^{\mathrm{inc}}_n\right)$. Additionally, define the source density matrix $\mathbf{Q}$, with the elements represented as $Q_{ln}=q_l\left(\widehat{\mathbf{x}}^{\mathrm{inc}}_n\right)$, therefore, we have the following relationship:

$$\mathbf{S}=\mathbf{C}^{ff}\mathbf{Q}. \tag{4}$$

The vectors $\mathbf{S}_{ex}$, $\mathbf{Q}_{ex}$, and $\mathbf{C}_{ex}$ are expressed as

$$\mathbf{S}_{ex} = [\mathrm{S}_{11},\mathrm{S}_{12},...,\mathrm{S}_{1n},\mathrm{S}_{21},\mathrm{S}_{22},...,\mathrm{S}_{2n},...,\mathrm{S}_{m1},\mathrm{S}_{m2},...,\mathrm{S}_{mn}]^{\mathrm{T}}, \tag{5}$$

$$\mathbf{Q}_{ex} = [\mathrm{q}_{11},\mathrm{q}_{12},...,\mathrm{q}_{1n},\mathrm{q}_{21},\mathrm{q}_{22},...,\mathrm{q}_{2n},\cdots,\mathrm{q}_{m1},\mathrm{q}_{m2},...,\mathrm{q}_{mn}]^{\mathrm{T}}, \tag{6}$$

$$\mathbf{C}_{ex} = [\mathbf{C}^1_e,\mathbf{C}^2_e,...,\mathbf{C}^m_e]^{\mathrm{T}}, \tag{7}$$

$$\mathbf{C}^i_e = \begin{bmatrix}\mathbf{C}_i & 0 & \cdots & 0\\ 0 & \mathbf{C}_i & \cdots & 0\\ \vdots & \vdots & \ddots & \vdots\\ 0 & 0 & \cdots & \mathbf{C}_i\end{bmatrix}, \tag{8}$$

where, the matrix element $\mathbf{S}$ corresponds to the acoustic pressure, $\mathbf{C}$ to the transfer function, and q to the source density function.

The sound scattering matrix $\mathbf{S}$ is an $m\times n$ matrix, the sound scattering transfer matrix $\mathbf{C}^{ff}$ is an $m\times l$ matrix, and the source density matrix $\mathbf{Q}$ is an $l\times n$ matrix. The sound scattering transfer matrix can be computed using the Gaussian–Legendre quadrature method for numerical integration. The sound scattering matrix $\mathbf{S}$ and the source density function matrix $\mathbf{Q}$ can be rewritten as column vectors $\mathbf{S}_{ex}$ and $\mathbf{Q}_{ex}$, respectively. Simultaneously, the matrix $\mathbf{C}^{ff}$ undergoes a matrix transformation to yield $\mathbf{C}_{ex}$:

$$\mathbf{S}_{ex}=\mathbf{C}_{ex}\mathbf{Q}_{ex}. \tag{9}$$

According to the principle of acoustic reciprocity, the ratio of the excitation applied at point A to the response at point B is equal to the ratio of the excitation applied at point B to the response at point A. The elements of the sound scattering matrix satisfy:

$$\mathbf{S}_{mn}=\mathbf{S}_{nm}. \tag{10}$$

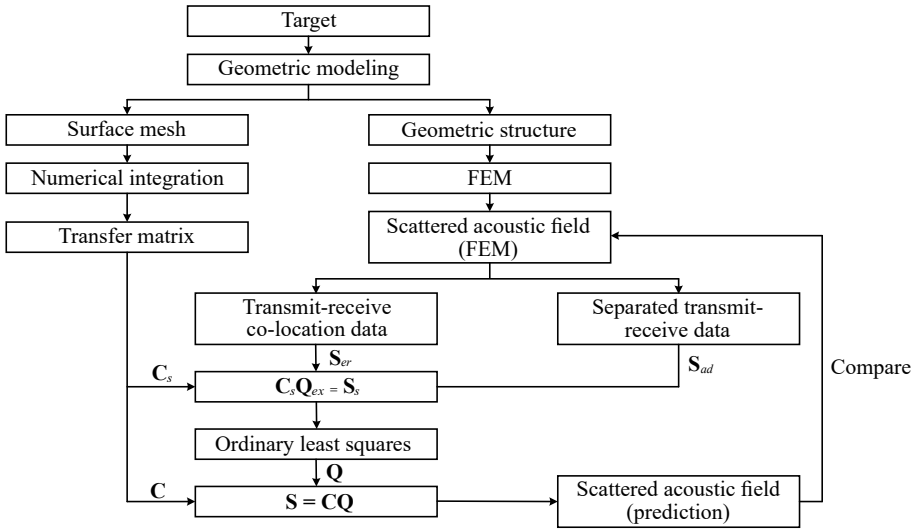

Fig. 2. Flow chart for calculating.

For the bistatic scattering matrix $\mathbf{S}$, it is a symmetric matrix where the upper triangular elements are equal to the lower triangular elements. By performing elimination while retaining the diagonal elements, $m_1(m_1+1)/2$ equations are obtained:

$$\mathbf{S}_{re} = \mathbf{C}_{re}\mathbf{Q}_{re}, \tag{11}$$

where $\mathbf{S}_{re}$ is composed of the monostatic scattered acoustic pressure and a zero vector.

Assuming that the monostatic acoustic scattering matrix $\mathbf{S}_{re}$ is known, a portion of the scattered sound pressure data $\mathbf{S}_{ad}$ from the receive-transmit separated configuration is added to the vector $\mathbf{S}_{re}$. At the same time, the corresponding row vector in the matrix $\mathbf{C}_{ex}$ that corresponds to $\mathbf{S}_{ad}$ is found. These are then combined to form the matrix $\mathbf{C}_{ad}$, which is subsequently appended to the matrix $\mathbf{C}_{re}$. This results in a sound scattering matrix $\mathbf{S}_s$ that contains both monostatic and partial bistatic configurations, as well as the corresponding matrix $\mathbf{C}_s$ is:

$$\mathbf{S}_s = \begin{bmatrix} \mathbf{S}_{re} \\ \mathbf{S}_{ad} \end{bmatrix}, \qquad \mathbf{C}_s = \begin{bmatrix} \mathbf{C}_{re} \\ \mathbf{C}_{ad} \end{bmatrix}. \tag{12}$$

The least squares method is used to approximate the solution of Eq. (6), resulting in the source density matrix $\mathbf{Q}_{ex}$. The obtained column vector $\mathbf{Q}_{ex}$ is then transformed into an $l_1 \times n_1$ matrix $\mathbf{Q}$. This matrix $\mathbf{Q}$, along with the calculated bistatic scattering transfer matrix $\mathbf{C}_{ml}^{ff}$, is substituted into Eq. (3) to obtain the bistatic scattered sound pressure $\mathbf{S}$. The detailed procedure is illustrated in Fig. 2.

The target strength is calculated using the following expression, assuming an incident acoustic pressure of 1 Pa:

$$\mathrm{TS} = 20\log(\mathrm{abs}(\mathbf{S}_s)). \tag{13}$$

To evaluate how much input data is required to achieve accurate prediction results, the ratio η between the elements of the input scattered sound pressure data and the predicted scattered sound pressure data can be expressed as

$$\eta = \frac{k(k+1)+2m_1}{2m_1^2 - k(k+1) - 2m_1} \times 100\,\%. \tag{14}$$

3. Case studies

The finite element software COMSOL Multiphysics, a multi-physics coupling software, is used to solve the scattering sound field under planar wave incidence. Partial sound scattering data obtained from simulation calculations and the target surface mesh are used as input to predict the separated transmit-receive scattering sound field. Finally, the prediction results are compared and analyzed with the finite element results.

3.1. Cylinder

Figure 3 is a schematic diagram of the triangular mesh model for column targets. The acoustic scatter-

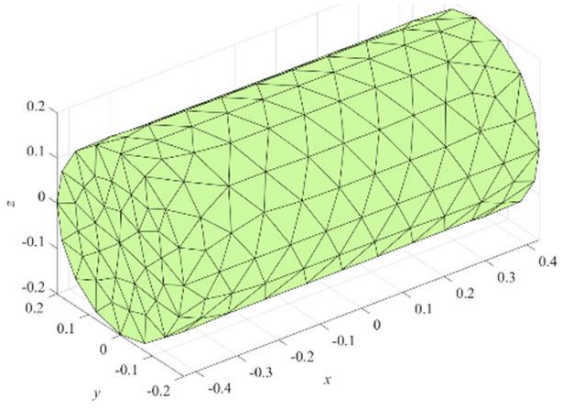

Fig. 3. Cylindrical target surface geometry mesh model.

ing transfer function is calculated according to the grid model $\mathbf{C}_{ml}^{ff}$, the calculation frequency is 100 Hz–1 kHz, the step length is 50 Hz, the incidence angle and receiving angle are 0°–360°, and the step length is 2°, different quantities of finite element calculation data are taken as input for prediction.

According to the grid model, the calculation conditions for the sound scattering transfer function remain consistent with those described earlier. Predictions are performed using varying amounts of finite element simulation data as input. Bistatic target strength predictions for cylindrical targets are conducted using a rigid cylinder as shown in Fig. 4.

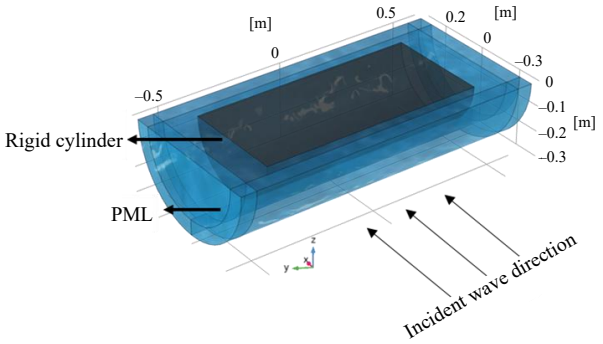

Fig. 4. Schematic diagram of rigid cylinder COMSOL modelling.

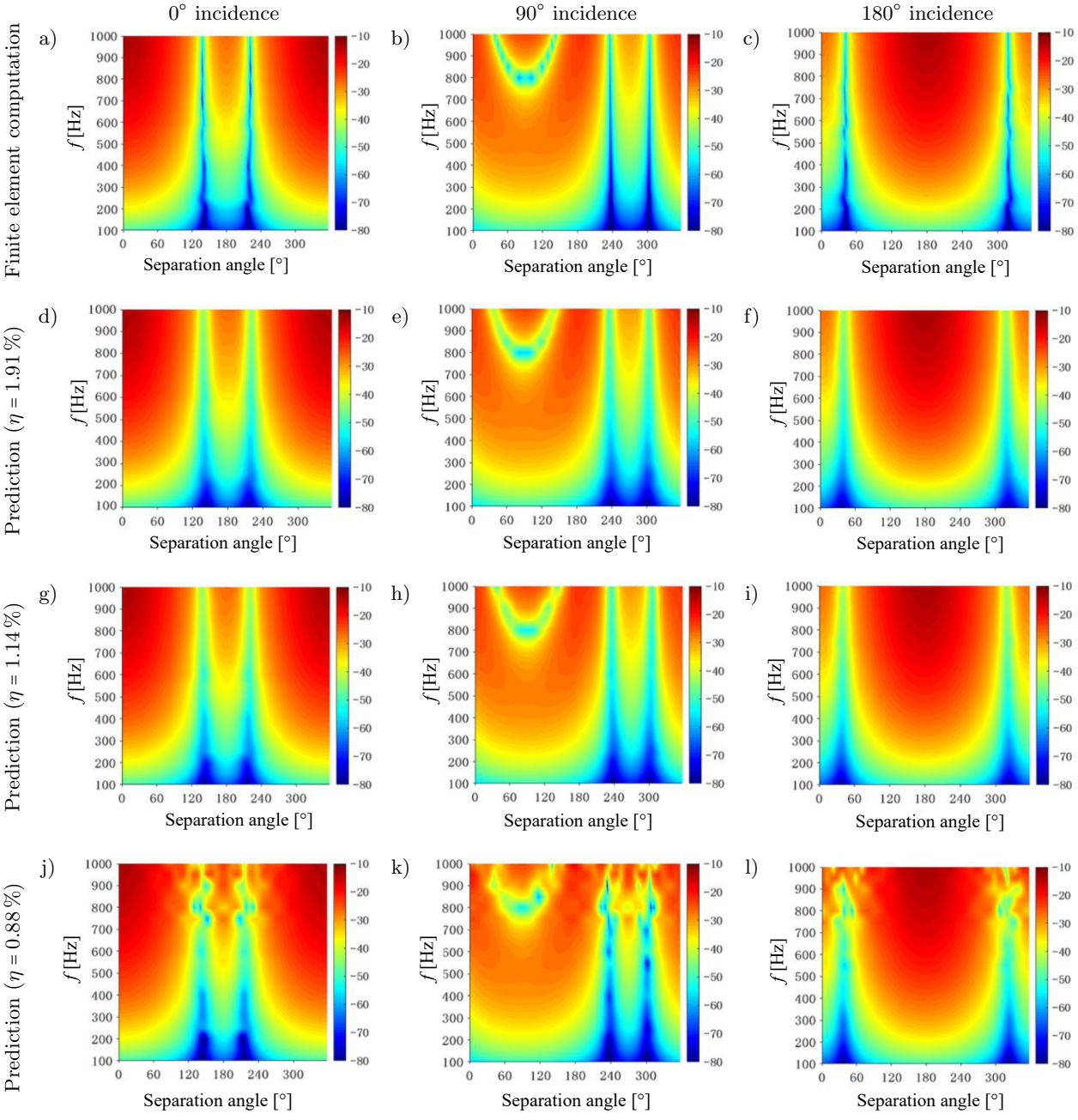

Fig. 5. Comparison of frequency-angle spectra of rigid cylinder predictions and FEM target strength.

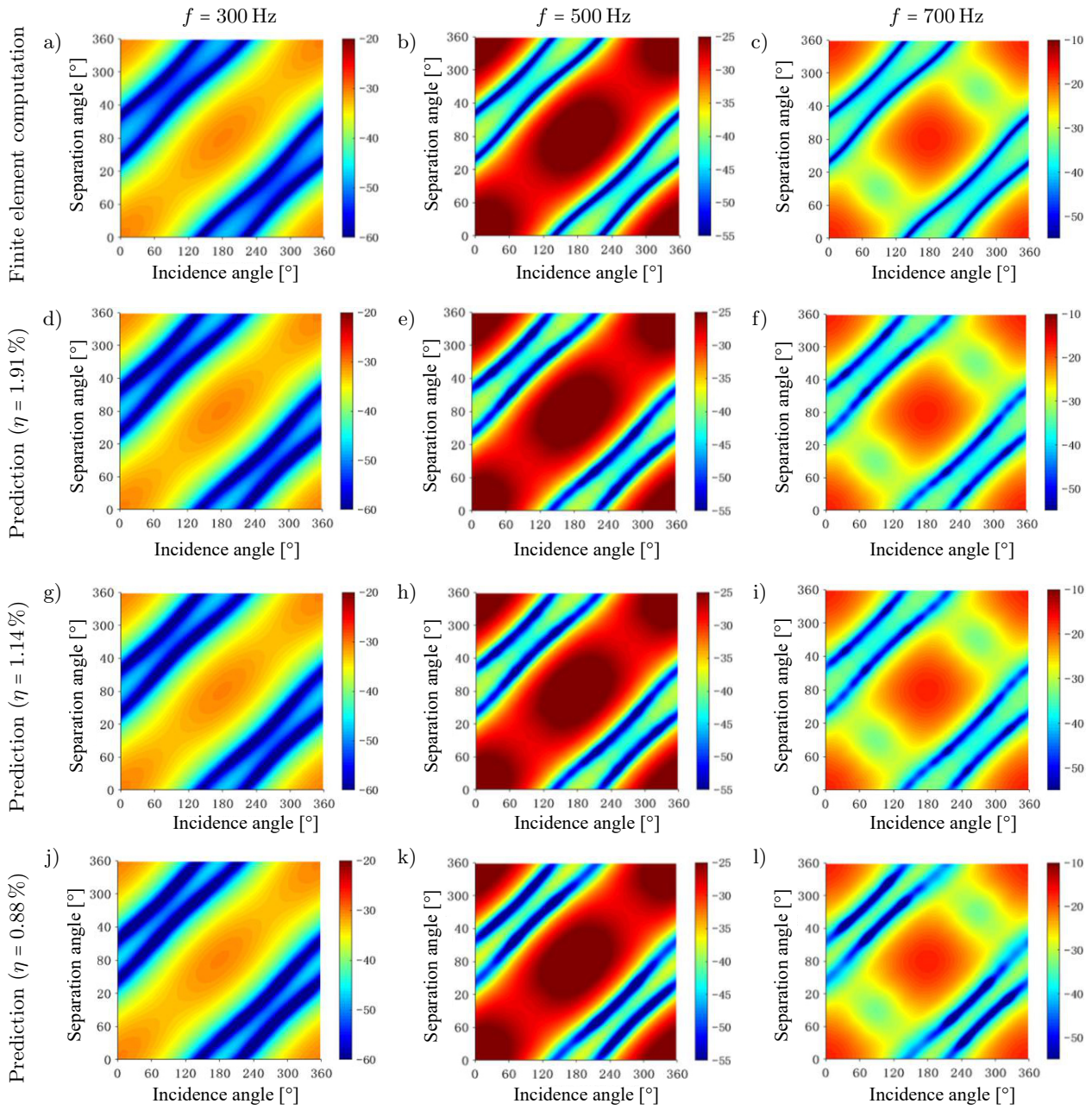

Fig. 6. Prediction of rigid cylindrical target strength maps and calculation using the finite element method for separate transmission and reception.

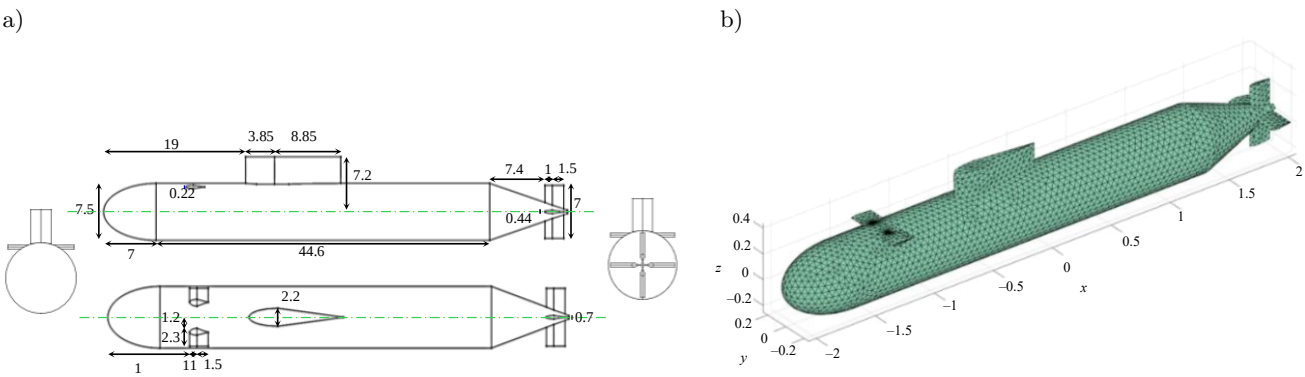

Fig. 7. Benchmark single-hull submarine model:
a) schematic diagram of the geometric model; b) surface mesh models.

The bistatic scattering sound field matrix **S** is constructed by sorting out the finite element calculation results, the bistatic scattered sound field is predicted by controlling the ratio η of the input element and the prediction element. Figure 5 shows the comparison results of the target strength frequency-angle spectrum between forecast results and finite element calculation results. Figure 6 compares the target strength predicted by the proposed method and the finite element method under different incident and receiving angles.

3.2. Benchmark model

The applicability of the method discussed in this paper is examined by selecting the Benchmark single-shell model, which has a total length of 62 m. The specific dimensions are shown in Fig. 7.

The underwater vehicle model is subjected to the finite element simulation, where the hull is set as rigid. The incident wave is a harmonic plane wave with unit amplitude in the xOy plane. The calculation conditions are the same as those for the cylinder.

As shown in Fig. 8, the predicted results for the Benchmark scaled model are similar to the prediction trends for the cylindrical model. As the number of input elements increases, the predicted results become more consistent with the analytical solution. However, the prediction accuracy decreases as the frequency increases. Figure 8 presents the bistatic target strength maps for the Benchmark scaled model and the FEM; Figs. 8a–8c show the finite element results, Figs. 8d–8f present the predicted results for $\eta = 3.15\,\%$; and Figs. 8g–8i show the predicted results for $\eta = 1.91\,\%$. Figure 9 compares the predicted and finite element computed bistatic target strength maps for the Benchmark scaled model.

4. Conclusion

This paper presents a prediction method for bistatic scattering sound fields based on limited data. The bistatic scattering sound field is expressed as the product of the target's sound scattering transfer function and the source density function. The target surface mesh is used as input to numerically integrate

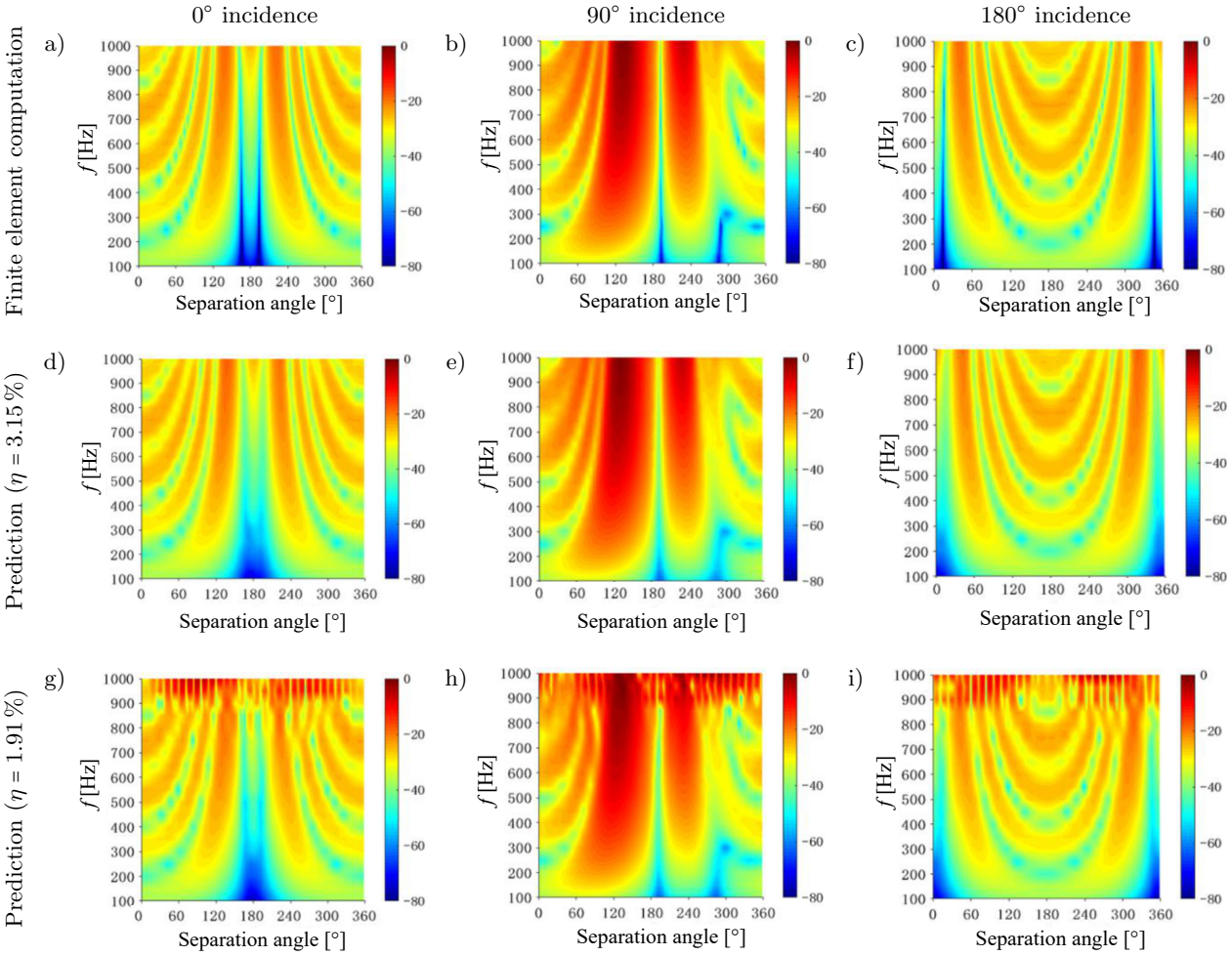

Fig. 8. Comparison of the predicted and finite element target strength frequency-angle spectra for the Benchmark scaled model.

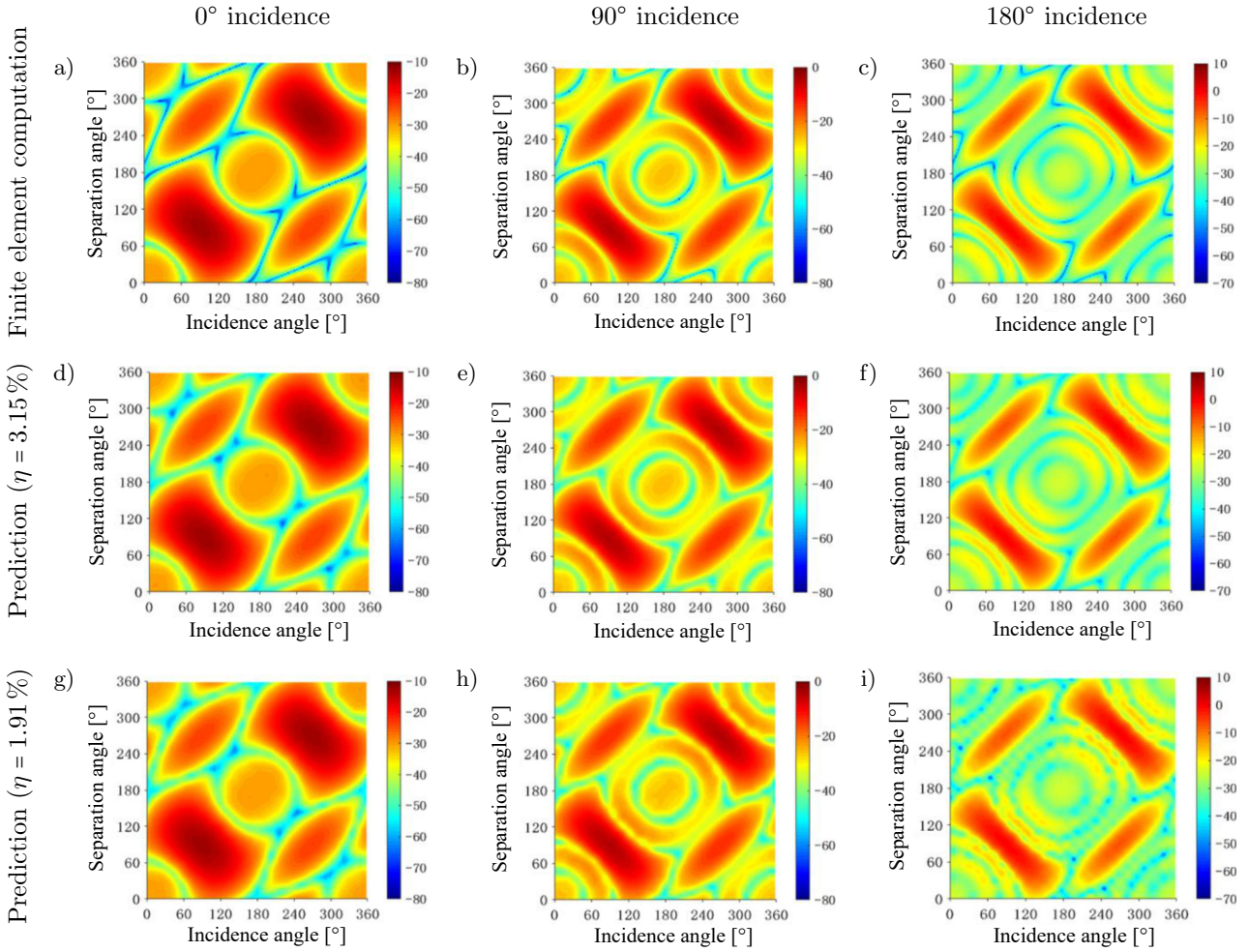

Fig. 9. Comparison of the predicted and finite element computed bistatic target strength maps for the Benchmark scaled model.

and obtain the bistatic target sound scattering transfer function. Using the known co-located transmit-receive scattered sound pressure, n sets of separated transmit-receive scattered sound pressures, and their corresponding sound scattering transfer functions as input, the source density function is solved using the least squares method. This method establishes a connection between single-base and bistatic scattering sound fields, offering significant practical value in acoustic scattering experiments, numerical calculations, and underwater countermeasure applications. The proposed prediction method has the following features:

1) This prediction method is applicable to low-frequency bistatic scattering sound field forecasting. In theory, it can be used to calculate the scattering sound field for any complex target model without relying on the internal structure of the target. It only requires the input of the surface geometric mesh and known scattered sound pressure data to predict the bistatic scattering sound field for targets with complex structures. The method demonstrates good computational efficiency for low-frequency, small target bistatic scattering sound field calculations.
2) The prediction accuracy of this method is dependent on both the precision and location of the input elements. The higher the precision of the input elements, the more accurate the prediction. Additionally, the location of the input elements has a significant impact on the prediction accuracy. When the known input elements correspond to the peaks of the scattering sound field, the prediction performs better. For bistatic scattering sound fields, the strongest scattered echoes typically occur in the forward scattering direction of the target, while strong echoes are also found in the backscattering direction, i.e., the co-located transmit-receive direction. Furthermore, scattering echoes from the mirrored reflection directions are also significant. In contrast, the scattering echo in the vertical direction of the incident wave is relatively weak. Therefore, using elements from these directions as known data for prediction results in higher computational efficiency.

3) The method proposed in this paper estimates the target strength of any complex shape and structure at any given angle of view based on a small amount of known data. It can be used for the engineering prediction of bistatic target strength for complex underwater targets and is applicable in underwater bistatic experiments. This method only requires the target surface mesh, making the modeling process simple and the calculation speed relatively fast, which holds certain potential application value in numerical calculations and underwater countermeasures. However, this method is suitable for low-frequency bistatic scattering sound field prediction, and the accuracy of the predictions is dependent on the position and precision of the input elements.

Fundings

This research did not receive any specific grant from funding agencies in the public, commercial, or not-for-profit sectors.

Conflict of interest

The authors declare that they have no known competing financial interests or personal relationships that could have appeared to influence the work reported in this paper.

References

1. Agounad S., Décultot D., Chati F., Léon F., Khandouch Y. (2023), Experimental study of the bistatic acoustic scattering from cylindrical shell, *Mechanical Systems and Signal Processing*, **186**: 109892, https://doi.org/10.1016/j.ymssp.2022.109892.
2. Chen C.X., Peng Z.L., Song H., Xue Y.Q., Zhou F.L. (2024), Prediction method of the low-frequency multistatic scattering sound field for underwater spherical targets based on limited data [in Chinese], *Journal of Shanghai Jiaotong University*, **58**(7): 1006–1017.
3. Cheng G., Zhang M., Du K., Yao W. (2010), Model and experiments for bistatic scattering strength of underwater objects, [in:] *2010 International Conference on Computer Application and System Modeling (ICCASM 2010)*, **9**: V9-489-V9-492, https://doi.org/10.1109/ICCASM.2010.5622985.
4. Fan J., Zhou L.K. (2006), Graphical acoustics computing method for echo characteristics calculation of underwater targets [in Chinese], *Acta Acustica*, **31**(6): 511–516.
5. Gu R., Peng Z., Xue Y., Xu C., Chen C. (2025), An improved fast prediction method for full-space bistatic acoustic scattering of underwater vehicles, *Sensors*, **25**(8): 2612, https://doi.org/10.3390/s25082612.
6. Gunderson A.M., España A.L., Marston P.L. (2017), Spectral analysis of bistatic scattering from underwater elastic cylinders and spheres, *The Journal of the Acoustical Society of America*, **142**(1): 110–115, https://doi.org/10.1121/1.4990690.
7. Liu Y.C., Zhang M.M., Wang Y.L. (2012), Calculation of target bistatic acoustic scattering using physical acoustic method [in Chinese], *Journal of Naval University of Engineering*, **24**(4): 101–103.
8. Long L.Y, Zhao H.S, Li D. (2022), Analysis of array configuration design for multi-base sonar buoy systems, *Acoustics and Electronics Engineering*, **2022**(1): 6–9.
9. Meng Z.R., Song Y., Yu F.X., Zhang C.L., Zhang Y.Q. (2024), Highlight model of underwater target acoustic scattering in the bistatic system, *Journal of Computers*, **35**(2): 231–249, http://doi.org/10.53106/199115992024043502015.
10. Park S.H. *et al.* (2006), Bistatic scattering from a hemi-spherically capped cylinder, *The Journal of the Acoustical Society of Korea*, **25**(3E): 115–122.
11. Peng Z.L., Wang B., Fan J. (2018), Simulation and experimental studies on acoustic scattering characteristics of surface targets, *Applied Acoustics*, **137**: 140–147, https://doi.org/10.1016/j.apacoust.2018.02.014.
12. Schenck H.A., Benthien G.W., Barach D. (1995), A hybrid method for predicting the complete scattering function from limited data, *The Journal of the Acoustical Society of America*, **98**(6): 3469–3481, https://doi.org/10.1121/1.413779.
13. Schmidt H. (2001), Bistatic scattering from buried targets in shallow water, [in:] *Proceedings, GOATS 2000 Conference*, La Spezia, **2001**: 21–22.
14. Schneider J.B., Wagner C.L., Broschat S.L. (1998), Implementation of transparent sources embedded in acoustic finite-difference time-domain grids, *The Journal of the Acoustical Society of America*, **103**(1): 136–142, https://doi.org/10.1121/1.421084.
15. Tang W.L., Fan J., Ma Z.C. (2018), *Acoustic Scattering of Underwater Targets* [in Chinese], Beijing: Science Press.
16. Wang B., Wang W.H., Fan J., Zhao K.Q., Zhou F.L., Tan L.W. (2022), Modeling of bistatic scattering from an underwater non-penetrable target using a Kirchhoff approximation method, *Defence Technology*, **18**(7): 1097–1106, https://doi.org/10.1016/j.dt.2022.04.008.
17. Waterman P.C. (2005), New formulation of acoustic scattering, *The Journal of the Acoustical Society of America*, **45**(6): 1417–1429, https://doi.org/10.1121/1.1911619.
18. Xue Y.Q., Peng Z.L., Yu Q., Zhang C., Zhou F., Liu J. (2023), Analysis of acoustic scattering characteristics of underwater targets based on Kirchhoff approximation and curved triangular mesh [in Chinese], *Acta Armamentarii*, **44**(8): 2424–2431.
19. Zhang L.L., Yang R.J., Yang C.Y. (2011), Research on underwater maneuvering target tracking technology [in Chinese], *Technical Acoustics*, **30**(1): 68–73, https://doi.org/10.3969/j.issn1000-3630.2011.01.012.
20. Zhou L.K, Fan J., Tang W.L. (2009), Analyzing acoustic scattering of elastic objects using coupled FEM-BEM technique [in Chinese], *Journal of Shanghai Jiaotong University*, **43**(8): 1258–1261.